

Hadronic description of nuclear matter and neutron star properties

Yao Ma,^{1,*} Yong-Liang Ma,^{1,†} and Jia-Ying Xiong^{2,1,‡}

¹*School of Frontier Sciences, Nanjing University, Suzhou 215163, China*

²*School of Fundamental Physics and Mathematical Sciences,
Hangzhou Institute for Advanced Study, UCAS, Hangzhou 310024, China*

(Dated: March 3, 2026)

The composition of the neutron star is one of the most fundamental and long-standing problems in nuclear- and astro-physics. The known properties of nuclear matter, together with the astronomical observations, impose the stringent and interconnected constraints on the theoretical descriptions. In this work, by using the most general quantum hydrodynamics model including σ, ω, ρ and a_0 in addition to nucleons, and performing a Bayesian joint analysis of experimental nuclear matter data and astrophysical observations, we point out that the nuclear matter made of only hadrons can provide a unified description of nuclear matter properties and astrophysical observations at 1σ -level. In addition, we find that the existence of $\sigma\omega\rho a_0$ interaction naturally leads to a peak structure in the speed of sound at $\sim (2-3)$ times saturation density n_0 which results to a small size intermediate mass neutron star and the upper bound mass $\sim 2M_\odot$. What we find here indicate that the sequential measurement of neutron star mass and radius by the next generation facilities, especially that of the intermediate mass neutron stars, is crucial for distinguishing the pure nucleonic stars from the hybrid ones.

Introduction— The properties of dense nuclear matter (NM) especially that relevant to the cores of massive neutron stars (NSs) have been studied for several decades but there are still several fundamental questions, for example, the composition of the matter, are waiting for clarification. The observation of massive NSs [1, 2] and the detection of gravitational wave (GW) stemming from the binary NS merger [3] further motivated the interests in this direction [4–6]. The clarification of these questions is crucial for understanding the nuclear force, the deconfinement phase transition, the evolution of compact stars as well as the GWs for the ground based facilities.

The observations of massive NSs around $2M_\odot$ [1, 2] with M_\odot being the solar mass indicate that the equation of state (EoS) of compact star matter should be stiff and sound velocity (SV) favors a peak structure at medium density [7]. However, the measurement of PSR J0030+0451 [8] and PSR J0437-4715 [9], and especially PSR J0614-3329 [10], have collectively shrink the radii of the intermediate mass NS and substantially soften the EoS at intermediate densities. This tension makes it increasingly challenging to satisfy all observational constraints simultaneously within theoretical frameworks. Moreover, the nuclear physics experiments, such as the heavy-ion collisions (HICs) and the analysis of nuclei structures [11–22], have already provided valuable constraints on the properties of NM around saturation density $n_0 \approx 0.16 \text{ fm}^{-3}$.

In the microscopic description of NM, it is natural to take hadrons—baryons and mesons—as the explicit degrees of freedom (DoFs) at low density. However, at high densities, i.e., $\gtrsim 2n_0$, the situation is quite unclear since it is naively argued that the overlaps between nucleons cannot be overlooked. In literature, for various purposes and intuitions, the compact star matter are preconceived as

quark matter [4], quarkyonic matter [23, 24], color-flavor-locked matter [25, 26], topology objects [27, 28], as well as the pure hadronic matter [29, 30] to be discussed in this work. Even in the hadronic matter description, a plenty of modifications have been made for various purpose, for example, including the $a_0(980)$ (δ resonance), ρ - ω mixing, σ - ρ mixing, etc, for specific purposes. Therefore, it is crucial to clarify whether the simplest approach, here the hadronic description, can saturate all the constraints from nuclear experiments and astro-observations before going to models with exotic DoFs.

To complete our motivation, we consider the most general quantum hydrodynamics (GQHD) model including σ, ρ, ω and a_0 in addition to nucleons, written up to dimension-4. The parameters in the model are estimated by using the Bayesian joint analysis (BJA) with respect to the NM properties and astrophysical observations at 1σ -level. We find that the pure hadronic description can yield the NM properties and NS observations including the most stringent constraint PSR J0614-3329 at 1σ -level, and generate a peak structure in the SV at intermediate densities, without resorting to any transitions from hadron to exotic configurations. Due to the peak structure of SV which partitions the EoS to soft and stiff segments, the NSs with intermediate mass have smaller radii, consistent with PSR J0614-3329, but maximum mass of NS is about $2M_\odot$, supporting the massive NS.

The model— We consider the most GQHD that incorporates all the hadron resonances below 1 GeV, e.g., σ, ω, ρ and a_0 mesons, as well as the nucleons. We will not consider pion in the Lagrangian since it vanishes in the relativistic mean field (RMF) approximation. Up to dimension-four, the model takes the form

$$\mathcal{L} = \mathcal{L}_N + \mathcal{L}_\sigma + \mathcal{L}_\omega + \mathcal{L}_\rho + \mathcal{L}_{a_0} + \mathcal{L}_I, \quad (1)$$

where

$$\begin{aligned}
\mathcal{L}_N &= \bar{\Psi} (i\gamma^\mu \partial_\mu - m_N) \Psi , \\
\mathcal{L}_\sigma &= \frac{1}{2} (\partial_\mu \sigma \partial^\mu \sigma - m_\sigma^2 \sigma^2) - \frac{1}{3} g_2 \sigma^3 - \frac{1}{4} g_3 \sigma^4 \\
&\quad - \frac{1}{2} g_4 \sigma^2 \omega^\mu \omega_\mu - \frac{1}{2} g_5 \sigma^2 \vec{\rho}^\mu \cdot \vec{\rho}_\mu \\
&\quad - g_6 \sigma \vec{\rho}^\mu \cdot \vec{\rho}_\mu - g_7 \sigma \omega^\mu \omega_\mu , \\
\mathcal{L}_\omega &= -\frac{1}{4} \Omega^{\mu\nu} \Omega_{\mu\nu} + \frac{1}{2} m_\omega^2 \omega^\mu \omega_\mu + \frac{1}{4} c_3 (\omega^\mu \omega_\mu)^2 \\
&\quad + \frac{1}{2} c_4 \omega^\mu \omega_\mu \vec{\rho}^\mu \cdot \vec{\rho}_\mu , \\
\mathcal{L}_\rho &= -\frac{1}{4} \vec{P}^{\mu\nu} \cdot \vec{P}_{\mu\nu} + \frac{1}{2} m_\rho^2 \vec{\rho}^\mu \cdot \vec{\rho}_\mu + \frac{1}{4} d_3 (\vec{\rho}^\mu \cdot \vec{\rho}_\mu)^2 , \\
\mathcal{L}_{a_0} &= \frac{1}{2} \partial_\mu \vec{a}_0 \cdot \partial^\mu \vec{a}_0 - m_{a_0}^2 \vec{a}_0 \cdot \vec{a}_0 + \frac{1}{4} b_3 (\vec{a}_0 \cdot \vec{a}_0)^2 \\
&\quad + \frac{1}{2} b_4 (\vec{a}_0 \cdot \vec{a}_0) (\vec{\rho}^\mu \cdot \vec{\rho}_\mu) + \frac{1}{2} b_5 \sigma (\vec{a}_0 \cdot \vec{a}_0) \\
&\quad + \frac{1}{2} b_6 \vec{a}_0 \cdot \vec{a}_0 \sigma^2 + \frac{1}{2} b_7 \vec{a}_0 \cdot \vec{a}_0 \omega^\mu \omega_\mu + b_8 \vec{a}_0 \cdot \vec{\rho}^\mu \omega_\mu \sigma \\
&\quad + b_9 \vec{a}_0 \cdot \vec{\rho}_\mu \omega^\mu , \\
\mathcal{L}_I &= \bar{\Psi} (g_\sigma \sigma - g_\omega \gamma^\mu \omega_\mu - g_\rho \gamma^\mu \vec{\rho}_\mu + g_{a_0} \vec{a}_0) \Psi . \quad (2)
\end{aligned}$$

In the model, $\Psi = (p, n)^T$ is the iso-doublet of nucleon field, $\vec{\rho}_\mu = \rho_\mu^i \tau^i$, $\vec{a}_0 = a_0^i \tau^i$, and $\Omega^{\mu\nu} = \partial^\mu \omega^\nu - \partial^\nu \omega^\mu$ and $\vec{P}^{\mu\nu} = \partial^\mu \vec{\rho}^\nu - \partial^\nu \vec{\rho}^\mu$ are field strength tensors of the corresponding vector mesons.

The energy density \mathcal{E} can be obtained by using the standard RMF approach and, therefore, the pressure P via $P = -\mathcal{E} + n \frac{d\mathcal{E}}{dn}$. Then the NS mass-radius (M-R) relation can be obtained by solving the Tolman-Oppenheimer-Volkoff (TOV) equation with the calculated EOS of beta-equilibrium nuclear matter. Additionally, the EoS of the NS crust is considered by interpolating to the standard BPS EoS [31] below $0.5n_0$ [32].

Considering the well determined masses of mesons and nucleons [33], we set $m_\omega = 782$ MeV, $m_\rho = 763$ MeV, $m_{a_0} = 980$ MeV, and $m_N = 939$ MeV in the numerical process. The mass of σ meson is less certain due to its broad width and strong coupling to pions, so we vary it from 400 to 800 MeV. By using the lessons from the chiral nuclear force models [34–37], we limit the couplings $g_\sigma, g_\omega, g_\rho$ and g_{a_0} within $(-20, 20)$. From literature [38–40], the magnitudes of three-meson couplings and four-meson couplings are taken to be less than 10000 MeV and 1000, respectively. Then, the 21-dimensional parameter set θ to be estimated includes: $g_\sigma, g_\omega, g_\rho, g_{a_0}, b_i, c_3, c_4, g_j, d_3$ with $(i = 3, \dots, 9, j = 2, \dots, 7)$, and m_σ .

The Bayesian analysis— The Bayesian analysis provides a systematic framework to incorporate various constraints from nuclear physics experiments and astrophysical observations based on Bayes' theorem [41],

$$p(\theta | \mathbf{D}) = \frac{p(\mathbf{D} | \theta)p(\theta)}{p(\mathbf{D})} , \quad (3)$$

where θ denotes the model parameters, $p(\theta)$ is the prior distribution encoding theoretical expectations and empirical knowledge about the parameters before considering any data, $p(\mathbf{D} | \theta)$ is the likelihood function quantifying the compatibility between the model predictions and the data, and $p(\mathbf{D})$ is the Bayesian evidence serving as a normalization constant. $p(\mathbf{D})$ is defined as

$$p(\mathbf{D}) = \int p(\mathbf{D} | \theta)p(\theta)d\theta . \quad (4)$$

With the assumption that the different data are independent, the overall likelihood can be written as the product of the likelihood for each individual data:

$$p(\mathbf{D} | \theta) = \prod_{i=1}^n p(D_i | \theta) . \quad (5)$$

In this work, the data \mathbf{D} consists of two parts: the NM properties and the M-R relations of NSs. More specifically, we will consider the constraints from the binding energy $E(n)$, pressure $P(n)$, incompressibility $K(n)$, symmetry energy $E_{\text{sym}}(n)$, and slope of symmetry energy $L(n)$ around saturation density n_0 . For the M-R relations, under the Gaussian assumption, we obtain the constraints at 1σ -level from Refs. [2, 3, 8–10, 42, 43]. It should be noted that the contribution of M-R relation to the Eq. (5) is estimated by choosing the maximum value of a M-R line predicted by the model for a given constraints. Within the BJA framework discussed in detail in App. A, NM properties and NS M-R observations are incorporated into a unified likelihood, allowing the model parameters to be constrained in a statistically consistent manner.

NM properties and NS structure— By using the BJA discussed above, we perform the assessment of model (1). For comparison, we also consider several widely used Walecka-type models, including TM1 [44], NL1 [45], NL3 [46], FSU- $\delta 6.7$ [47], FSUGold [48].

From Tab. I and Fig. 1 one can clearly observe that, the general model (1) can saturate all the constraints from experimental data and astro-observations. This observation results to a conclusion that the pure-hadronic model can undoubtedly yield the EoSs that saturates all the existing NM properties and the observed astrophysical M-R ranges, no compelling motivation to resort to exotic DoFs, such as the confinement phase transition.

If one were focus on the NM properties, all the considered models roughly saturate the constraints, as shown in Tab. I. However, the M-R relation predicted by the Walecka-type models fail to cover all credible astrophysical regions at 1σ level as shown in Fig. 1, indicating the residual tension between the NM systematics and the astrophysical data. In contrast, the GQHD considered, with parameter sets GQHD1 and GQHD2, can reproduce all the constraints. This is because of some terms, such as the $\sigma\omega a_0\rho$ interaction to be discussed later, included in

TABLE I. Nuclear matter properties at saturation density. Higher (\uparrow) BJA indicate better overall agreement between model predictions and empirical data. BJA is defined in Eq. (9).

	Empirical	TM1	NL1	NL3	FSU- $\delta 6.7$	FSUGold	GQHD1	GQHD2
$E(n_0)$	-16.0 ± 1.0 [19]	-16.2	-16.5	-16.3	-16.3	-16.3	-17.2	-16.1
n_0	0.16 ± 0.05 [19]	0.142	0.152	0.148	0.148	0.148	0.159	0.155
$E_{\text{sym}}(n_0)$	30.9 ± 1.9 [49]	36.0	43.5	38.2	32.7	29.1	32.3	33.4
$L(n_0)$	52.5 ± 17.5 [50]	108	140	121	53.5	53.1	49.6	49.6
$K(n_0)$	230 ± 30 [51]	257	207	246	229	228	349	214
$E(1.5n_0)$	-13.3 ± 0.5 [52]	-13.0	-13.1	-12.6	-13.3	-13.5	-12.5	-13.3
$P(1.5n_0)$	3.41 ± 1.29 [53]	4.26	5.52	5.57	3.97	3.58	6.52	3.67
$L(\frac{2}{3}n_0)$	71.5 ± 22.6 [54]	69.6	85.0	74.3	54.5	39.2	69.9	55.2
m_σ	600 ± 200 [33]	511	492	503	492	492	445	504
BJA	\uparrow	-4.51	-15.3	-11	3.8	4.28	1.13	8.03

the model. The values of the parameters in sets GQHD1 and GQHD2 are given in Tab. II in App. A.

From Fig. 1 one may find that the size of the NS with intermediate mass, $\approx (1.3 - 1.5)M_\odot$, is significant for revealing the constituents of NM. A smaller radius, like PSR J0614-3329, may be in tension to most of the pure hadronic description. To obtain a smaller radius, the EoS

should be soft, equivalently, a smaller SV to be discussed later, at intermediate density. Consequently, more attractive force is need. However, to predict a larger maximum NS mass, the EoS should be stiff. In a word, to consistent with the observations, the EoS should be soft at intermediate density but stiff high density relevant to the cores of massive stars.

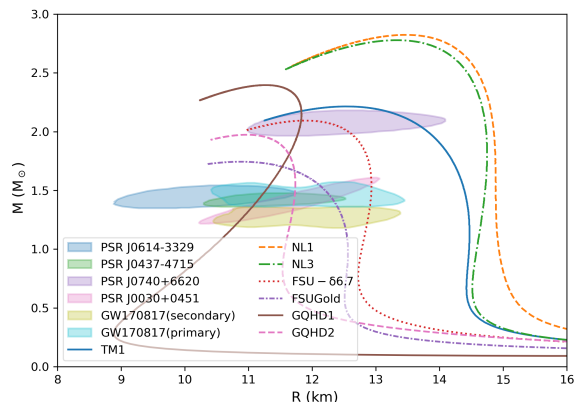


FIG. 1. The M-R relation of TM1 [44], NL1 [45], NL3 [46], FSU- $\delta 6.7$ [47], FSUGold [48], GWM1 and GWM2 with CBC. The constraints PSR J1614-2230, PSR J0348+0432, PSR J0740+6620, J0030+0451, PSR J0437-4715, and PSR J0614-3329, from [3, 8-10, 42, 43, 55].

We finally consider the EoSs from various of models and compare them with the constraints from HIC [15], χEFT [56] and Kaons constraint [57, 58] in Fig. 2. One can see that, at low densities, $\chi EFT - N^2LO$ cannot put too much constraints on the models considered but $\chi EFT - N^3LO$ and Kaons constraint disagree with NL1, NL3. More stringent constraints comes from HIC. One can easily see that both GQHD2 and FSUGold fall into the constraint band well. This is consistent with the BJA

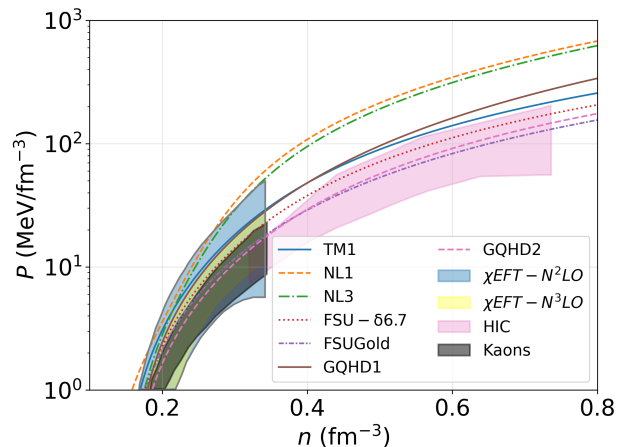


FIG. 2. Pressure as a function of density for symmetric NM. HIC constraint is from $Au + Au$ flow-data analysis [15], $\chi EFT - N^2LO$ and $\chi EFT - N^3LO$ are from chiral nuclear force [56], Kaons constraint is from [57, 58].

given in Tab. I. Since the EoS from GQHD2 is stiffer than that from FSUGold, the maximum mass of NS obtained from the former is bigger than that from the latter and is about $2M_\odot$, agree with the observation of massive NSs, as illustrated in Fig. 1.

Sound velocity— Let us consider the SV $v_s^2 = dP/d\varepsilon$ in medium, which reflects the stiffness of the EoS. The

results of GQHD and the compared Walecka-type models are shown in Fig. 3.

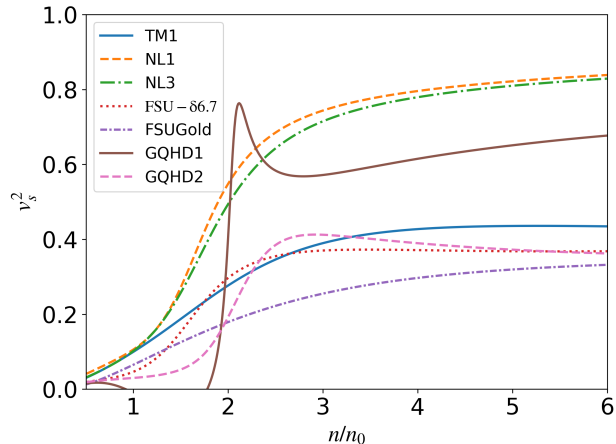


FIG. 3. The density dependence of sound velocity v_s^2 from different models.

Interestingly, the results in Fig. 3 show that both the parameter sets GQHD1 and GQHD2 yield a pronounced peak in the density dependence of v_s^2 . This observation reaffirms our previous conclusion that the peak of SV can arise in pure hadronic models [59, 60]. This is due to the b_8 term, the $\sigma\omega a_0\rho$ interaction, significantly affect the speed of sound and the M-R relation under charge neutrality and β -equilibrium conditions, as shown in Fig. 4. Nevertheless, the non-monotonic evolution of the sound speed implies that the EoS becomes effectively softer or stiffer over different density intervals, that is, the EoS is softer at lower density which stiffer at high densities. This non-monotonic behavior indicates that the resulted radius of NS is smaller at intermediate mass while the maximum mass could be large, say $\sim 2M_\odot$. This conclusion is supported by the M-R relations from other models in the figure. As a result, the sequential measurement of NSs with different masses are crucial for diagnosing the microscopic composition of NS matter.

From Fig. 3, one can see that, NL1 and NL3 models yield roughly the largest SV, therefore the stiffest EoS and consequently the largest maximum values of the NS mass and biggest NS radii, as shown in Fig. 1. The EoS is too stiff to yield the smaller NS radii that consistent with the observations.

Tidal deformability— We finally consider another independent constraint from astrophysics, the tidal deformability (TD). Here, we consider the TD inferred from GW170817 which was firstly estimated to be $\Lambda_{1.4} \leq 800$ [3] and then stringent to $\Lambda_{1.4} = 190_{-120}^{+390}$ [42] for NS with mass $1.4M_\odot$. We refer to the later as the constraint. In addition, the correlations between TD and lighter NS (C1) and heavier NS (C2) of the binary system at 50% credible level are also plotted [42, 61, 62].

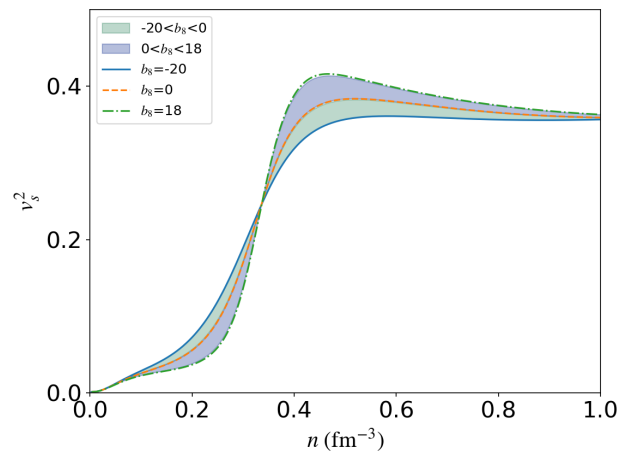


FIG. 4. Effect of the mixed $\sigma\omega\rho a_0$ coupling on the v_s^2 .

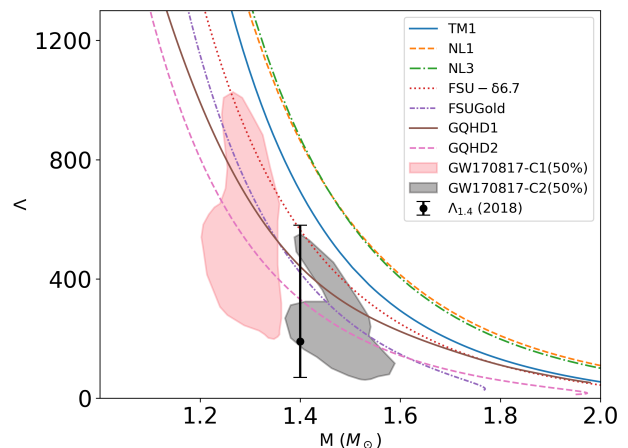


FIG. 5. Tidal deformability as a function of mass obtained from various models.

From Fig. 5 one can conclude that, all predictions of GQHD, FSU- $\delta 6.7$ and FSUGold fail in the constraints, both $\Lambda_{1.4}$ and the correlation region. Explicitly, the GQHD predicts $\Lambda_{1.4} = 441.6$ for GQHD1 and $\Lambda_{1.4} = 320.5$ for GQHD2. Therefore, the smaller TD may gives a more stringent constraint on the hadronic model.

Conclusion and outlook— In this work, by using the most general Quantum Hadrodynamics (GQHD) model written up to dimension-4 incorporating all the hadrons below 1 GeV, i.e., $\sigma, \omega, \rho, a_0$, and n, p , we clarified that all the data from nuclear physics experiments and astrophysics observations can be saturated and, consequently, there is no sufficient reason to introduce exotic DoFs, such as quark matter, quarkyonic matter, and so on.

To systematically estimate the deviation from the constraints, we introduced the BJA framework, a statistically rigorous method that enables a quantitative and

unified assessment of model performance across different parameter sets by jointly incorporating nuclear and astrophysical constraints at 1σ level. Within this framework, we find that the parameter set GQHD2 exhibits superior overall performance compared with the other considered models.

Our results indicate that the smaller size of intermediate mass NSs may give a strong constraint on the NS EoS. In such a case, a stronger attractive force between nucleons is needed, and consequently a soft EoS or smaller SV. However, to obtain the massive mass NS around $2M_\odot$, the EoS must be stiff enough above the central density of the intermediate mass of NS. Therefore a peak structure of SV should exist which was naturally predicted in the present GQHD. This implies that the sequential measurement of neutron star mass and radius by the next generation facilities, especially that of the intermediate mass neutron stars, is crucial for diagnosing the pure nucleonic stars.

In the literature, there are several other preconceived composition of compact star matter, such as the quarky-

onic matter and quark matter. These structures are widely discussed and results of the models are consistent with observations more or less. Therefore, it is significant to investigate the boundary of these structures, including the present one, to give the precision of the measurement and novel signal to distinguish different structures, and to pin down the location of the hadron-exotic structure if the latter exists.

The last issue we want to address is that the present GQHD is the pure phenomenological one. No full attention has been paid to the fundamental symmetries of QCD, such as chiral symmetry that has been recognized to control the dynamics of hadron processes. This is another point deserving future exploration.

Acknowledgments—The work of Y. M. is supported by Jiangsu Funding Program for Excellent Postdoctoral Talent under Grant Number 2025ZB516. Y. L. M. is supported in part by the National Science Foundation of China (NSFC) under Grant No. 12547104, the National Key R&D Program of China under Grant No. 2021YFC2202900 and Gusu Talent Innovation Program under Grant No. ZXL2024363.

Appendix A. Bayesian joint analysis

Based on Bayes' theorem, our primary interest lies in the posterior distribution $p(\theta | \mathbf{D})$ with θ being the parameter space and \mathbf{D} being the distribution of the data. Since the evidence term $p(\mathbf{D})$ is independent of the model parameters θ , it can be treated as a normalization constant, thus neglected in parameter inference. Consequently, by using Eq.(5), Eq.(3) can be rewritten as:

$$p(\theta | \mathbf{D}) \propto \prod_{i=1}^n p(D_i | \theta) p(\theta). \quad (6)$$

We further assume a Gaussian likelihood for $p(\mathbf{D} | \theta)$, corresponding to the normally distributed observational errors. In the absence of prior preference, uniform priors are adopted for all parameters within their allowed ranges.

Under the above assumptions, the posterior distribution is fully determined by the Gaussian likelihood. To ensure comparable contributions from observables with vastly different magnitudes and experimental uncertainties, all data are transformed into a normalized residual space by shifting the experimental central values to zero and rescaling the corresponding uncertainties to a common effective value $\Delta = 0.5$. Explicitly, for each observable we define:

$$\widetilde{M}_i(\theta) = \frac{\Delta}{\sigma_i^{\text{exp}}} [R_i(\theta) - D_i^{\text{exp}}] \quad (7)$$

where D_i^{exp} and σ_i^{exp} denote the experimental central value and associated uncertainty of the i -th observable, respectively, and $R_i(\theta)$ represents the corresponding model prediction. The likelihood for each observable can then be written as

$$p(D_i | \theta) = \frac{1}{\sqrt{2\pi}\Delta} \exp\left(-\frac{\widetilde{M}_i^2(\theta)}{2\Delta^2}\right). \quad (8)$$

This procedure effectively weights each observable by its relative deviation from the experimental value, rather than by its absolute scale, thereby preventing datasets with large numerical magnitudes or uncertainties from dominating the inference. The posterior distribution is then evaluated using a Gaussian likelihood in this normalized space.

Finally, to avoid numerical overflow arising from the product of likelihood terms, particularly in regions of high likelihood, we define BJA as:

$$\text{BJA} = \ln \left(\prod_{i=1}^n p(D_i | \theta) p(\theta) \right). \quad (9)$$

Appendix B. BJA and parameter space

Following Eq. (9), the optimal parameter set was found and listed in Tab. II, and corresponding values of BJA has already been listed in Tab. I. Then, to show the geometry of parameter space around reference value in Tab. II, we take

TABLE II. The estimated values of model parameters. $m_\sigma, b_5, b_9, g_2, g_6$ and g_7 are in unit of MeV.

Parameter	TM1	NL1	NL3	FSU- $\delta 6.7$	FSUGold	GQHD1	GQHD2
$g_{\sigma NN}$	10.0	-10.1	-10.1	-10.2	-10.6	7.55	-9.90
$g_{\omega NN}$	12.6	13.3	12.8	13.4	14.3	10.5	12.5
$g_{\rho NN}$	4.63	4.98	4.57	7.27	5.88	5.97	7.05
$g_{a_0 NN}$	—	—	—	-6.70	—	-6.60	-6.25
m_σ	511	492	503	492	492	445	504
b_5	—	—	—	—	—	-124	117
b_9	—	—	—	—	—	-1820	-10.6
g_2	-1420	2400	2130	1600	844	-676	1710
g_6	—	—	—	—	—	-1960	32.5
g_7	—	—	—	—	—	-36.6	136
b_3	—	—	—	—	—	254	72.1
b_4	—	—	—	—	—	2.07	2.26
b_6	—	—	—	180	—	5.26	181
b_7	—	—	—	—	—	-6.43	0.117
b_8	—	—	—	—	—	-328	17.7
g_3	0.610	-36.3	-30.1	5.88	49.9	7.58	6.59
g_4	—	—	—	—	—	-2.87	1.19
g_5	—	—	—	—	—	123	0.949
c_3	71.3	—	—	172	418	1.09	172
c_4	—	—	—	204	2590	0.127	204
d_3	—	—	—	—	—	648	4.68

the g_ρ as an example and show the result in Fig. 6. In this analysis, each parameter is allowed to vary independently within a $\pm 20\%$ range around its reference value (red dots, local maximum of BJA) in order to examine the resulting correlations. Overall, the correlation patterns can be classified into two categories as demonstrated in Fig. 6: (i) parameters that exhibit clear correlations with g_ρ such as $g_\sigma, g_\omega, g_{a_0}$ and m_σ , and (ii) the remaining parameters that show little or correlation.

Meanwhile, within the Bayesian framework, we are able to quantitatively establish the relationship between the model parameters and physical observables: As illustrated in the Fig. 7, the curves represent the correlations between the coupling constant g_ω and the nuclear matter properties $n_0, E(n_0), L(n_0), K(n_0), E_{sym}(n_0)$, while the color bar indicates the result of the BJA (the lighter colors correspond to the larger BJA values), as well as corresponding correlation between g_ω and the M-R relation.

* mayao@nju.edu.cn

† ylma@nju.edu.cn

‡ xiongjiaying21@mails.ucas.ac.cn

-
- [1] P. Demorest, T. Pennucci, S. Ransom, M. Roberts, and J. Hessels, Shapiro Delay Measurement of A Two Solar Mass Neutron Star, *Nature* **467**, 1081 (2010).
 - [2] J. Antoniadis et al., A Massive Pulsar in a Compact Relativistic Binary, *Science* **340**, 6131 (2013).
 - [3] B. P. Abbott et al. (LIGO Scientific, Virgo), GW170817:

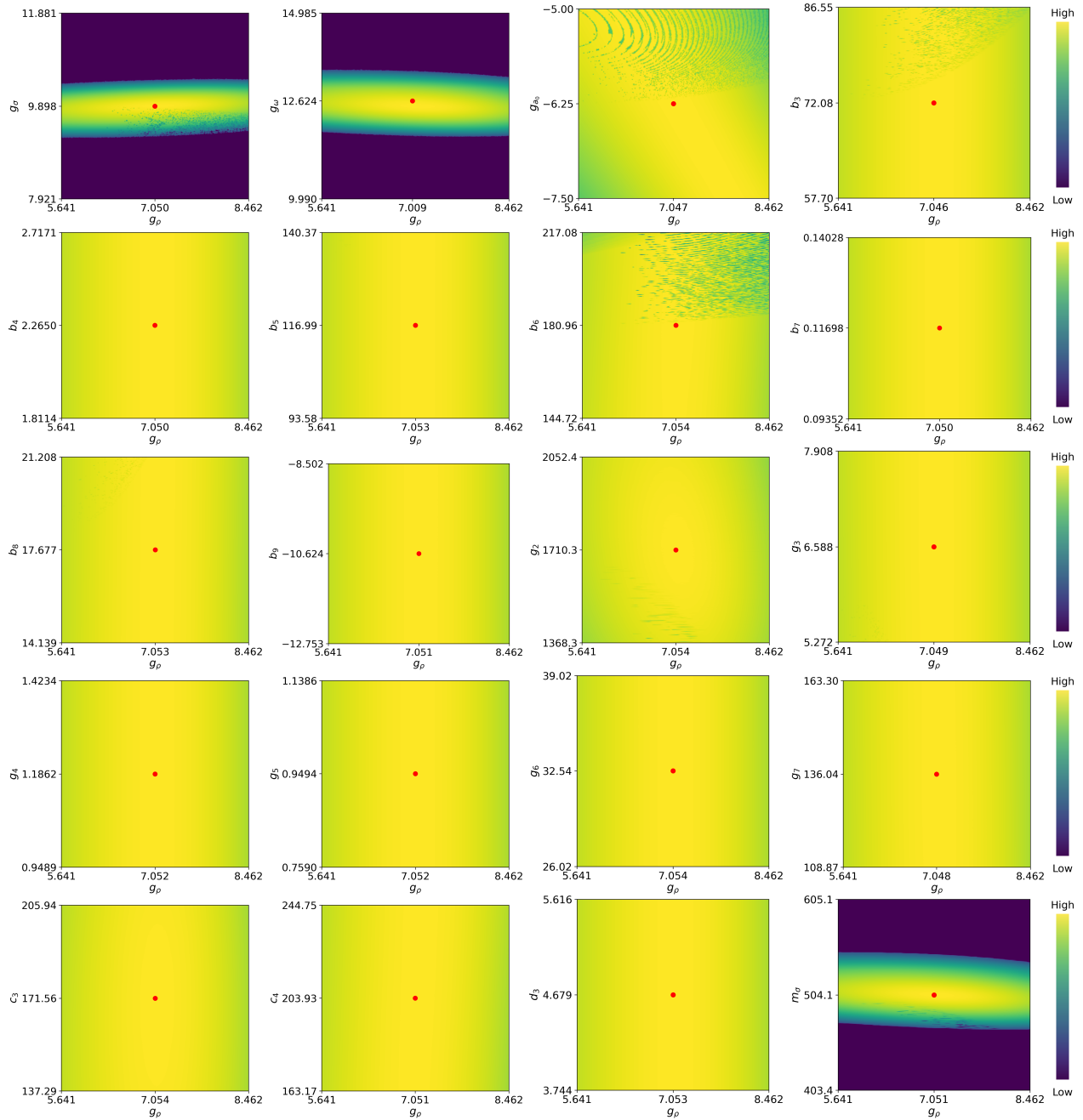


FIG. 6. The correlation between $g_{\rho NN}$ and other parameters in GQHD. Colors represent the relative magnitudes of BJA , and red dots represent our parameters.

- Observation of Gravitational Waves from a Binary Neutron Star Inspiral, *Phys. Rev. Lett.* **119**, 161101 (2017).
- [4] G. Baym, T. Hatsuda, T. Kojo, P. D. Powell, Y. Song, and T. Takatsuka, From hadrons to quarks in neutron stars: a review, *Rept. Prog. Phys.* **81**, 056902 (2018), arXiv:1707.04966 [astro-ph.HE].
- [5] E. Annala, T. Gorda, A. Kurkela, J. Nättilä, and A. Vuorinen, Evidence for quark-matter cores in massive neutron stars, *Nature Phys.* **16**, 907 (2020), arXiv:1903.09121 [astro-ph.HE].
- [6] Y.-L. Ma and M. Rho, Towards the hadron–quark conti-

- nity via a topology change in compact stars, *Prog. Part. Nucl. Phys.* **113**, 103791 (2020), arXiv:1909.05889 [nucl-th].
- [7] S. Altıparmak, C. Ecker, and L. Rezzolla, On the Sound Speed in Neutron Stars, *Astrophys. J. Lett.* **939**, L34 (2022), arXiv:2203.14974 [astro-ph.HE].
- [8] S. Vinciguerra et al., An Updated Mass–Radius Analysis of the 2017–2018 NICER Data Set of PSR J0030+0451, *Astrophys. J.* **961**, 62 (2024), arXiv:2308.09469 [astro-ph.HE].
- [9] D. Choudhury et al., A NICER View of the Nearest and

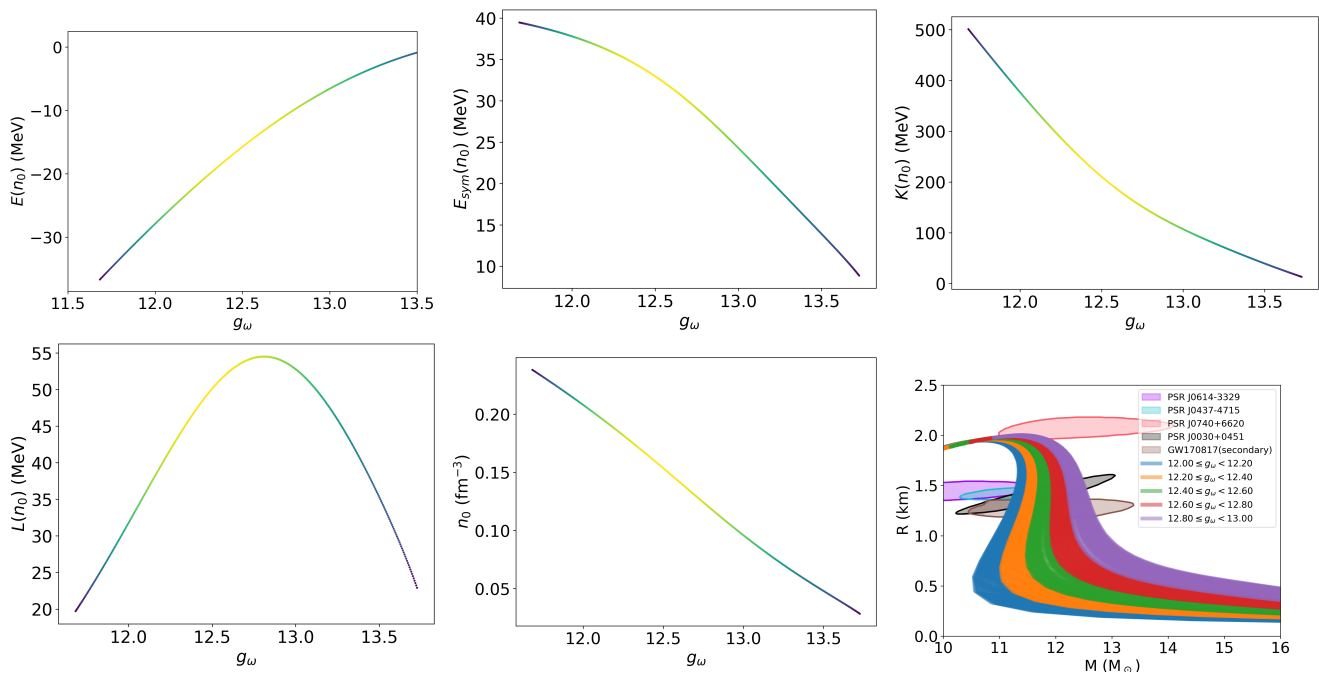


FIG. 7. The relation between g_ω and physical quantities.

- Brightest Millisecond Pulsar: PSR J0437–4715, *Astrophys. J. Lett.* **971**, L20 (2024), arXiv:2407.06789 [astro-ph.HE].
- [10] L. Mauviard et al., A NICER view of the 1.4 solar-mass edge-on pulsar PSR J0614–3329 (2025), arXiv:2506.14883 [astro-ph.HE].
- [11] D. H. Youngblood, H. L. Clark, and Y. W. Lui, Incompressibility of Nuclear Matter from the Giant Monopole Resonance, *Phys. Rev. Lett.* **82**, 691 (1999).
- [12] B. A. Brown, Neutron radii in nuclei and the neutron equation of state, *Phys. Rev. Lett.* **85**, 5296 (2000).
- [13] S. Karataglidis, K. Amos, B. A. Brown, and P. K. Deb, Discerning the neutron density distribution of Pb-208 from nucleon elastic scattering, *Phys. Rev. C* **65**, 044306 (2002), arXiv:nucl-th/0111020.
- [14] A. W. Steiner and B.-A. Li, Isospin diffusion in heavy-ion collisions and the neutron skin thickness of lead, *Phys. Rev. C* **72**, 041601 (2005), arXiv:nucl-th/0505051.
- [15] P. Danielewicz, R. Lacey, and W. G. Lynch, Determination of the equation of state of dense matter, *Science* **298**, 1592 (2002), arXiv:nucl-th/0208016.
- [16] T. Klahn et al., Constraints on the high-density nuclear equation of state from the phenomenology of compact stars and heavy-ion collisions, *Phys. Rev. C* **74**, 035802 (2006), arXiv:nucl-th/0602038.
- [17] B.-A. Li, L.-W. Chen, and C. M. Ko, Recent Progress and New Challenges in Isospin Physics with Heavy-Ion Reactions, *Phys. Rept.* **464**, 113 (2008), arXiv:0804.3580 [nucl-th].
- [18] P. Russotto et al., Results of the ASY-EOS experiment at GSI: The symmetry energy at suprasaturation density, *Phys. Rev. C* **94**, 034608 (2016), arXiv:1608.04332 [nucl-ex].
- [19] M. Dutra, O. Lourenço, S. S. Avancini, B. V. Carlson, A. Delfino, D. P. Menezes, C. Providência, S. Typel, and J. R. Stone, Relativistic Mean-Field Hadronic Models under Nuclear Matter Constraints, *Phys. Rev. C* **90**, 055203 (2014), arXiv:1405.3633 [nucl-th].
- [20] L.-W. Chen, C. M. Ko, B.-A. Li, and J. Xu, Density slope of the nuclear symmetry energy from the neutron skin thickness of heavy nuclei, *Phys. Rev. C* **82**, 024321 (2010), arXiv:1004.4672 [nucl-th].
- [21] Z. Zhang and L.-W. Chen, Bayesian inference of the symmetry energy and the neutron skin in Ca48 and Pb208 from CREX and PREX-2, *Phys. Rev. C* **108**, 024317 (2023), arXiv:2207.03328 [nucl-th].
- [22] Y. Huang, K.-X. Huang, Z.-X. Yang, X.-L. Tu, J.-N. Hu, J.-T. Zhang, and J.-F. Han, Constraint on symmetry energy slope using neutron skins of ^{48}Ca , ^{64}Ni , ^{124}Sn , and ^{208}Pb and its impact on neutron star radius*, *Chin. Phys.* **49**, 094005 (2025).
- [23] L. McLerran and R. D. Pisarski, Phases of cold, dense quarks at large $N(c)$, *Nucl. Phys. A* **796**, 83 (2007), arXiv:0706.2191 [hep-ph].
- [24] L. McLerran and S. Reddy, Quarkyonic Matter and Neutron Stars, *Phys. Rev. Lett.* **122**, 122701 (2019), arXiv:1811.12503 [nucl-th].
- [25] M. G. Alford and A. Sedrakian, Compact stars with sequential QCD phase transitions, *Phys. Rev. Lett.* **119**, 161104 (2017), arXiv:1706.01592 [astro-ph.HE].
- [26] A. Geißel, T. Gorda, and J. Braun, Color Superconductivity under Neutron-Star Conditions at Next-to-Leading Order, *Phys. Rev. Lett.* **135**, 211901 (2025), arXiv:2504.03834 [hep-ph].
- [27] W.-G. Paeng, T. T. S. Kuo, H. K. Lee, Y.-L. Ma, and M. Rho, Scale-invariant hidden local symmetry, topology change, and dense baryonic matter. II., *Phys. Rev. D* **96**, 014031 (2017), arXiv:1704.02775 [nucl-th].
- [28] Y.-L. Ma, H. K. Lee, W.-G. Paeng, and M. Rho, Pseudoconformal equation of state in compact-star matter

- from topology change and hidden symmetries of QCD, *Sci. China Phys. Mech. Astron.* **62**, 112011 (2019), arXiv:1804.00305 [nucl-th].
- [29] B. D. Serot and J. D. Walecka, The Relativistic Nuclear Many Body Problem, *Adv. Nucl. Phys.* **16**, 1 (1986).
- [30] B. D. Serot and J. D. Walecka, Recent progress in quantum hydrodynamics, *Int. J. Mod. Phys. E* **6**, 515 (1997), arXiv:nucl-th/9701058.
- [31] G. Baym, C. Pethick, and P. Sutherland, The Ground state of matter at high densities: Equation of state and stellar models, *Astrophys. J.* **170**, 299 (1971).
- [32] W. D. Arnett and R. L. Bowers, A Microscopic Interpretation of Neutron Star Structure, *Astrophys. J. Suppl.* **33**, 415 (1977).
- [33] S. Navas et al. (Particle Data Group), Review of particle physics, *Phys. Rev. D* **110**, 030001 (2024).
- [34] X.-L. Ren, K.-W. Li, L.-S. Geng, B.-W. Long, P. Ring, and J. Meng, Leading order relativistic chiral nucleon-nucleon interaction, *Chin. Phys. C* **42**, 014103 (2018), arXiv:1611.08475 [nucl-th].
- [35] D. Djukanovic, J. Gegelia, S. Scherer, and M. R. Schindler, N N scattering in higher-derivative formulation of baryon chiral perturbation theory, *Few Body Syst.* **41**, 141 (2007), arXiv:nucl-th/0609055.
- [36] L. Girlanda, S. Pastore, R. Schiavilla, and M. Viviani, Relativity constraints on the two-nucleon contact interaction, *Phys. Rev. C* **81**, 034005 (2010), arXiv:1001.3676 [nucl-th].
- [37] H. Polinder, J. Haidenbauer, and U.-G. Meissner, Hyperon-nucleon interactions: A Chiral effective field theory approach, *Nucl. Phys. A* **779**, 244 (2006), arXiv:nucl-th/0605050.
- [38] Y. Ma and Y.-L. Ma, Composition of scalar mesons and their effects on nuclear matter properties in an extended linear sigma model, *Phys. Rev. D* **112**, 054026 (2025), arXiv:2507.10049 [nucl-th].
- [39] P. Kovács, J. Takátsy, J. Schaffner-Bielich, and G. Wolf, Neutron star properties with careful parametrization in the vector and axial-vector meson extended linear sigma model, *Phys. Rev. D* **105**, 103014 (2022), arXiv:2111.06127 [nucl-th].
- [40] D. Parganlija, P. Kovacs, G. Wolf, F. Giacosa, and D. H. Rischke, Meson vacuum phenomenology in a three-flavor linear sigma model with (axial-)vector mesons, *Phys. Rev. D* **87**, 014011 (2013), arXiv:1208.0585 [hep-ph].
- [41] T. Bayes, An essay towards solving a problem in the doctrine of chances, *Philosophical Transactions of the Royal Society of London* **53**, 370 (1763).
- [42] B. P. Abbott et al. (LIGO Scientific, Virgo), GW170817: Measurements of neutron star radii and equation of state, *Phys. Rev. Lett.* **121**, 161101 (2018).
- [43] T. Salmi et al., The Radius of the High-mass Pulsar PSR J0740+6620 with 3.6 yr of NICER Data, *Astrophys. J.* **974**, 294 (2024), arXiv:2406.14466 [astro-ph.HE].
- [44] Y. Sugahara and H. Toki, Relativistic mean field theory for unstable nuclei with nonlinear sigma and omega terms, *Nucl. Phys. A* **579**, 557 (1994).
- [45] P.-G. Reinhard, M. Rufa, J. Maruhn, W. Greiner, and J. Friedrich, Nuclear ground-state properties in a relativistic meson-field theory, *Zeitschrift für Physik A Atomic Nuclei* **323**, 13 (1986).
- [46] G. A. Lalazissis, J. König, and P. Ring, A New parametrization for the Lagrangian density of relativistic mean field theory, *Phys. Rev. C* **55**, 540 (1997), arXiv:nucl-th/9607039.
- [47] F. Li, B.-J. Cai, Y. Zhou, W.-Z. Jiang, and L.-W. Chen, Effects of Isoscalar- and Isovector-scalar Meson Mixing on Neutron Star Structure, *Astrophys. J.* **929**, 183 (2022), arXiv:2202.08705 [nucl-th].
- [48] B. G. Todd-Rutel and J. Piekarewicz, Neutron-Rich Nuclei and Neutron Stars: A New Accurately Calibrated Interaction for the Study of Neutron-Rich Matter, *Phys. Rev. Lett.* **95**, 122501 (2005), arXiv:nucl-th/0504034.
- [49] J. M. Lattimer and Y. Lim, Constraining the Symmetry Parameters of the Nuclear Interaction, *Astrophys. J.* **771**, 51 (2013), arXiv:1203.4286 [nucl-th].
- [50] P. Danielewicz and J. Lee, Symmetry Energy II: Isobaric Analog States, *Nucl. Phys. A* **922**, 1 (2014), arXiv:1307.4130 [nucl-th].
- [51] M. Dutra, O. Lourenco, J. S. Sa Martins, A. Delfino, J. R. Stone, and P. D. Stevenson, Skyrme Interaction and Nuclear Matter Constraints, *Phys. Rev. C* **85**, 035201 (2012), arXiv:1202.3902 [nucl-th].
- [52] A. Le Fèvre, Y. Leifels, W. Reisdorf, J. Aichelin, and C. Hartnack, Constraining the nuclear matter equation of state around twice saturation density, *Nucl. Phys. A* **945**, 112 (2016), arXiv:1501.05246 [nucl-ex].
- [53] B. A. Brown, Constraints on the Skyrme Equations of State from Properties of Doubly Magic Nuclei, *Phys. Rev. Lett.* **111**, 232502 (2013), arXiv:1308.3664 [nucl-th].
- [54] B. T. Reed, F. J. Fattoyev, C. J. Horowitz, and J. Piekarewicz, Implications of PREX-2 on the Equation of State of Neutron-Rich Matter, *Phys. Rev. Lett.* **126**, 172503 (2021), arXiv:2101.03193 [nucl-th].
- [55] B. P. Abbott et al. (LIGO Scientific, Virgo, Fermi GBM, INTEGRAL, IceCube, AstroSat Cadmium Zinc Telluride Imager Team, IPN, Insight-Hxmt, ANTARES, Swift, AGILE Team, 1M2H Team, Dark Energy Camera GW-EM, DES, DLT40, GRAWITA, Fermi-LAT, ATCA, ASKAP, Las Cumbres Observatory Group, OzGrav, DWF (Deeper Wider Faster Program), AST3, CAAS-TRO, VINROUGE, MASTER, J-GEM, GROWTH, JAGWAR, CaltechNRAO, TTU-NRAO, NuSTAR, Pan-STARRS, MAXI Team, TZAC Consortium, KU, Nordic Optical Telescope, ePESTO, GROND, Texas Tech University, SALT Group, TOROS, BOOTES, MWA, CALET, IKI-GW Follow-up, H.E.S.S., LOFAR, LWA, HAWC, Pierre Auger, ALMA, Euro VLBI Team, Pi of Sky, Chandra Team at McGill University, DFN, ATLAS Telescopes, High Time Resolution Universe Survey, RIMAS, RATIR, SKA South Africa/MeerKAT), Multi-messenger Observations of a Binary Neutron Star Merger, *Astrophys. J. Lett.* **848**, L12 (2017), arXiv:1710.05833 [astro-ph.HE].
- [56] S. Huth et al., Constraining Neutron-Star Matter with Microscopic and Macroscopic Collisions, *Nature* **606**, 276 (2022), arXiv:2107.06229 [nucl-th].
- [57] W. G. Lynch, M. B. Tsang, Y. Zhang, P. Danielewicz, M. Famiano, Z. Li, and A. W. Steiner, Probing the Symmetry Energy with Heavy Ions, *Prog. Part. Nucl. Phys.* **62**, 427 (2009), arXiv:0901.0412 [nucl-ex].
- [58] C. Fuchs, Kaon production in heavy ion reactions at intermediate energies, *Prog. Part. Nucl. Phys.* **56**, 1 (2006), arXiv:nucl-th/0507017.
- [59] L.-Q. Zhang, Y. Ma, and Y.-L. Ma, Peak of sound velocity, scale symmetry, and nuclear force in baryonic matter, *Phys. Rev. C* **112**, L031001 (2025), arXiv:2410.04142 [nucl-th].

- [60] L.-Q. Zhang, Y. Ma, and Y.-L. Ma, Nuclear matter properties from chiral-scale effective theory including a dilatonic scalar meson*, *Chin. Phys.* **50**, 024108 (2026), arXiv:2412.19023 [nucl-th].
- [61] The LIGO Scientific Collaboration and The Virgo Collaboration, Ligo-p1800115-v12: Ligo document p1800115-v12, <https://dcc.ligo.org/LIGO-P1800115/public> (2018), LIGO Data Release, accessed 2026-02-23.
- [62] P. J. Kalita, T. Malik, T. Zhao, B. Kumar, and J. M. Lattimer, Observable Signatures of a Quarkyonic Phase in Neutron Stars (2025), arXiv:2510.23405 [nucl-th].